

RESEARCH ARTICLE

Comparison of physical quality assurance between Scanora 3D and 3D Accuitomo 80 dental CT scanners

Ahmed S. Ali^{1,2*}, Daren Fteita¹ and Jarmo Kulmala¹

¹Laboratory of Biophysics, Cell Biology and Anatomy, Institute of Biomedicine, University of Turku, Turku, Finland; ²Department of Pediatric Dentistry, Faculty of Dentistry, Benghazi University, Benghazi, Libya

Background: The use of cone beam computed tomography (CBCT) in dentistry has proven to be useful in the diagnosis and treatment planning of several oral and maxillofacial diseases. The quality of the resulting image is dictated by many factors related to the patient, unit, and operator.

Materials and methods: In this work, two dental CBCT units, namely Scanora 3D and 3D Accuitomo 80, were assessed and compared in terms of quantitative effective dose delivered to specific locations in a dosimetry phantom. Resolution and contrast were evaluated in only 3D Accuitomo 80 using special quality assurance phantoms.

Results: Scanora 3D, with less radiation time, showed less dosing values compared to 3D Accuitomo 80 (mean 0.33 mSv, SD \pm 0.16 vs. 0.18 mSv, SD \pm 0.1). Using paired *t*-test, no significant difference was found in Accuitomo two scan sessions ($p > 0.05$), while it was highly significant in Scanora ($p > 0.05$). The modulation transfer function value (at 2 lp/mm), in both measurements, was found to be 4.4%. The contrast assessment of 3D Accuitomo 80 in the two measurements showed few differences, for example, the grayscale values were the same (SD = 0) while the noise level was slightly different (SD = 0 and 0.67, respectively).

Conclusions: The radiation dose values in these two CBCT units are significantly less than those encountered in systemic CT scans. However, the dose seems to be affected more by changing the field of view rather than the voltage or amperage. The low doses were at the expense of the image quality produced, which was still acceptable. Although the spatial resolution and contrast were inferior to the medical images produced in systemic CT units, the present results recommend adopting CBCTs in maxillofacial imaging because of low radiation dose and adequate image quality.

Keywords: CBCT; image quality; resolution; contrast; radiation dose

*Correspondence to: Ahmed S. Ali, Department of Pediatric Dentistry, Faculty of Dentistry, Benghazi University, Benghazi, Libya, Email: ahsamu@utu.fi

Received: 31 March 2015; Revised: 14 May 2015; Accepted: 15 May 2015; Published: 18 June 2015

Cone beam computed tomography (CBCT) has been introduced mainly to overcome the insufficient image quality obtained for dental patients using conventional radiographic techniques and the relatively high dose associated with the use of systemic computed tomography (CT) scan; a new imaging technology has been developed and it is known as CBCT (Fig. 1) (2).

After the successful use of special CT equipment in a variety of medical fields, for example, angiography and mammography, the idea of devising a CT unit for dental imaging emerged in the 1980s and many attempts were then undertaken in Japan (3). The first models of CBCT were manufactured and presented in Italy in 1998 and then appeared in Japan (4, 5) followed by the US in 2001 (6).

Obviously, the name of this imaging modality denotes the conical geometry of the X-ray beam. The general design of a CBCT scan unit consists of, as in other CT models, a scanning gantry which is composed of a single X-ray source and a 2D panel detector.

In CBCT technology, two types of image receptors exist (7). The first constitutes a combination of scintillation screen composed of cesium iodide, intermingled with image intensifier, for example, phosphor (input and output layers), electron optics, attached to a sensor, that is, CCD. The scintillation screen fluoresces when it is hit by photons and the signal produced is strengthened and magnified by the image intensifier layer. The photons are converted into electrical signal by means of CCD and then sent to the monitor.

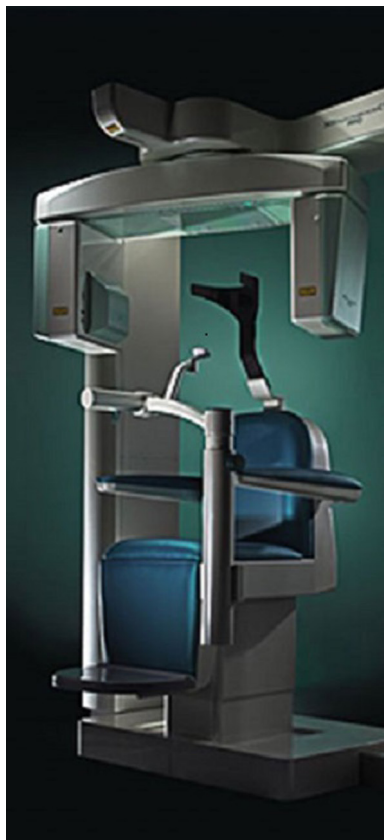


Fig. 1. A CBCT unit with a variable FOV (1).

Digital data can be reformatted in any form; this is known as multi-planar reformatting. For example, an image in the axial plane can be viewed in the sagittal plane and vice versa. Thin sections of CT images reveal more data than thicker ones, but forming thin sections would require higher dose and thus more radiation to the patient.

The fundamental geometrical difference between the conventional CT and CBCT is that the former scans the body in fan beam, making slices (or stacks) of it, while in CBCT the body is scanned in a cone-shape section. The cone-scanning pattern has the advantage of avoiding taking slices of the scanned object, thereby shortening the scanning time. It has proven its value in many branches of dentistry with regard to diagnosis (8) and treatment (9). Unlike the conventional CT units in which the patient has to be imaged in a supine position, patients undergoing CBCT imaging could be standing, in supine position, or seated with their chins resting on a chin-support seat in such a way that the cone beam covers the region of interest (ROI). When the patient is positioned properly, the imaging process starts by rotating the X-ray source and the panel detector around the patient so that a set of 2D projections is generated. The better image quality of the resulting image, including contrast and resolution, compared with the old-fashioned analogue radiography, maximizes the benefits of providing dental service to patients,

starting from correct diagnosis and ending in formulating a proper treatment plan.

Following the scanning process, reconstruction software processes the acquired 2D images, using special algorithms, to form a more advanced and complicated 3D image. The most commonly used reconstruction algorithm in CBCT imaging is a modified Feldkamp algorithm (10), which is a 3D adaptation of the filtered backprojection technique used in conventional CT with fan-beam geometry (11).

Optimum CT imaging is the ultimate goal of all radiologists because a high-quality image is very helpful in establishing a definitive diagnosis. Image quality can be assessed in two ways; either physically or psychologically (12). In this study, only physical assessment is undertaken in terms of evaluating the measured parameters: spatial resolution, contrast, and radiation dose.

Spatial resolution is the ability to distinguish two small structures, which are closely spaced and might otherwise appear as one object. In CT technology, resolution is assessed by means of gratings of line-pair phantoms (13). The modulation transfer function (MTF) is the customary parameter which has been adopted to evaluate the spatial resolution, because it can describe how the CT unit efficiently processes the signal (14). MTF calculates how the imaging device can detect a number of gratings arranged in a specific way (known as the spatial frequency).

Contrast is the difference in appearance of two adjacent structures due to their different reflection patterns of the incident light. In CT imaging, contrast is very important because it allows the diagnostician to recognize the different anatomical structures in a particular area of the body, especially if their attenuation coefficients are very close. Besides, it reflects the capacity of the display of an imaging device to receive the signals and reliably interpret them as gray or color outcome (15). Phantoms take a variety of figures for fulfilling the purpose of studying image contrast, and an example is shown in Figure 26 (16). The last measured parameter in this study was radiation dose, which has a profound effect on the image quality in such a way that increasing the dose improves the image quality. The reason behind this is that when more photons are beamed to an ROI (area of interest), the image noise is reduced and thus the image would be less grainy. The increase in X-ray dose is achieved by manipulating the mAs and kVp of the CT unit. Improving the image quality through raising the X-ray dose must be balanced with the consequences of over-exposing the patient during the scan procedure.

As in other parameters of image quality, radiation dose can be measured using specific phantoms, one of which is known as RANDO phantom.

The aim of the current work was to assess and compare quality assurance parameters between two dental CT units: Scanora 3D and 3D Accuitomo 80.

Materials and methods

Clinical CBCT units

Scanora 3D

Scanora 3D is a cone beam CT machine designed for making 3D images of maxillofacial structures. It is one of many imaging modalities manufactured by Soredex (Soredex Co., Tuusula, Finland) for providing the 3D form to the plain 2D dental radiographs. The unit is composed mainly of a motorized chair with a revolving scanner head fixed to a stand and a touch panel.

In its imaging, it has four fields of view (FOV): small (for small operations involving single tooth); medium (for viewing the whole jaw); large (for examining both jaws and TMJ) and extra-large (for imaging the entire maxillofacial area as well as airways).

Technical data of both Scanora 3D and 3D Accuitomo 80 (coming below) can be sought from their manufacturers' websites.

3D Accuitomo 80

The second clinical CT unit is included in this thesis for the purpose of comparison with Scanora is 3D Accuitomo 80 (J. Morita MFG. Corp., Kyoto, Japan). It provides super high-resolution 3D images of 80 μm sized voxel. In principle, it has the same basic components as Scanora but the general designs and formulation are different.

Quality assurance phantoms

Resolution phantoms

These are also known as image quality phantoms and their primary purpose, as the name denotes, is to evaluate the resolution power of the CT scan image. In this work, a wire phantom (X001-99520-400) was used to measure the spatial resolution of the 3D Accuitomo 80 CBCT. The wire is encased in a cylindrical phantom (Fig. 2) made of polymethylmethacrylate (PMMA).

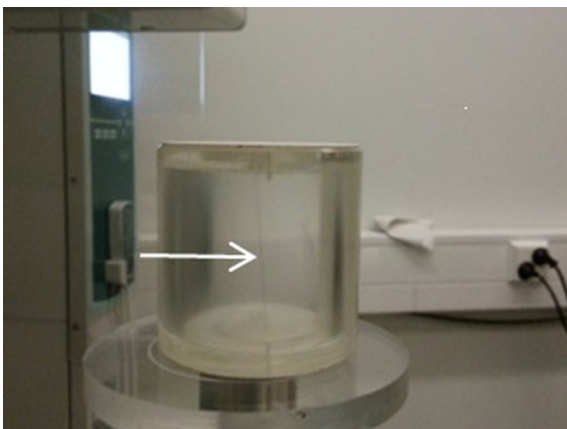


Fig. 2. A wire phantom, with the wire appearing vertical in the middle of the cylinder (arrow).

Contrast phantoms

In the measurement of CBCT image quality, contrast and resolution were assessed in the same session. Therefore, contrast phantoms used here are the same ones mentioned above in the section of resolution. These phantoms contained holes in the central axis which coincides with the phantom axis of rotation (17). Each hole can accommodate a PMMA rod used to aid in aligning the phantom within the CT gantry.

Dosimetry measurement tools

RANDO phantoms

The main purpose of anthropomorphic Rando[®] Alderson phantoms is to make the assessment of X-ray dosing in different locations inside the human head-like phantom. The measurement is done through insertion of small chips into drilled holes in a movable section which represents either the upper or lower jaw. In the present study, only the slices (levels) numbered 6 and 7 were assessed for X-ray dosimetry.

Thermoluminescent dosimeter chips

The radiation dose was measured using thermoluminescent dosimeters (TLD) chips.

They are made of lithium fluoride and have a lattice design (due to their crystalline nature) and the impurities in their structures act as ditches for trapping the free electrons after they are bounced off by the X-ray photons (when they are exposed to X-ray). For ease of identification, four pellets are set in a row inside special cards which are, in turn, slid into cassettes.

TLD reader

The radiation dose measured for both Scanora 3D and 3D Accuitomo 80 was read using Alnor TLD-System (ALNOR OY, Turku, Finland). This device loads the TLD chips (after lifting them from the slide card) into a measuring chamber where they are exposed to hot gas, that is, nitrogen.

The radiation doses calculated were average organ doses, and these were converted into effective doses as described already in the literature (18). This technique of measuring radiation dose by reading photons emitted from crystals as heated is called thermoluminescent dosimetry.

Details of defining the radiation dose

These chips were inserted into drilled holes in the RANDO phantom head and distributed throughout 12 locations (six holes of the same positions at two different levels: the lower jaw and one level below) (Fig. 3). The six chips were positioned in such a way that only one towards the anterior aspect (the chin side), two chips at the central horizontal axis (one on each side of the center), and the remaining three chips were located between the anterior and the middle sides.

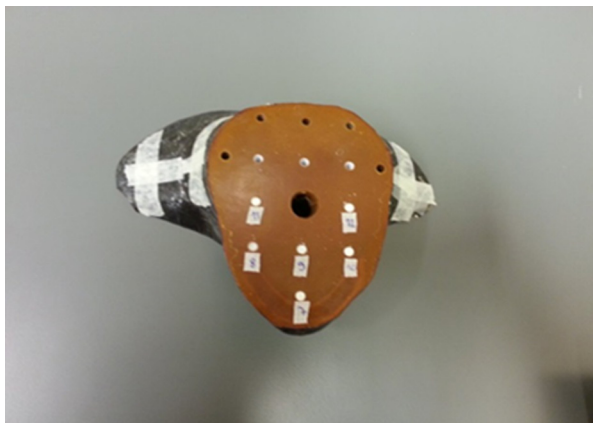


Fig. 3. The TLD chips inserted in their holes (from 1 to 6) in the slice, which was then fitted into the RANDO phantom.

All the statistical calculations in this study, including descriptive parameters and associations in the radiation dose values, were done in Excel (Microsoft Office 2010, Microsoft Co., Wa., USA).

The present work has been approved by Varsinais-(South-east Finland) Suomen Health Committee under the reference number 316/11.

Results

Image quality

The image quality was assessed using the two most important parameters: resolution and contrast. The measurements of image quality were done only on 3D Accuitomo 80. The measurements were conducted twice for each parameter using different settings.

Resolution

The first measurement was done at 90 kV and 6 mA while the FOV size was 60×60 .

The spatial resolution was determined using the mathematical concept of MTF. In the MTF graph, the image fidelity is charted against the number of line pairs that can be fit in a millimeter of space (lp/mm; spatial frequency) in the Y- and X-axes, respectively (Fig. 4). The MTF value was calculated after taking the average of radiating the object in eight directions. The maximum MTF value was found to be over 90% and it corresponded to a spatial frequency close to 1. The real object in the resolution phantom had a spatial frequency of 3 lp/mm (Fig. 4, upper right panel), but the reference for MTF assessment was set at 2 lp/mm and it was found to be 4.4% (Fig. 4, upper left panel). However, because this value is lower than the default standard (10% as shown in the Appendix), the measurement was repeated, but it was again lower, that is, 7.9%.

The second measurement was done at 80 kV and 7 mA while the FOV was kept the same, that is, 60×60 . The highest MTF value was about 54% and it corresponded

to a spatial frequency of <1 lp/mm. The reference for MTF assessment was set at 2 lp/mm and it was found to be 4.4% (Fig. 4, upper left panel). The same step was repeated for the sake of obtaining a higher value, but it was 7.9%.

During exposing the object to X-ray in both settings, the luminance signals were recorded and no artifacts, for example, streaking, were seen (Figs. 4 and 5, lower right panels).

Contrast

As with the resolution measurement, the contrast parameter (which comprised noise, uniformity/grayscale, and contrast resolution) was assessed for 3D Accuitomo 80 by conducting two measurements using different settings of the device.

The first measurement was done at 90 kV and 6 mA while the second was at 80 kV and 7 mA; the image mode (FOV size) was kept the same at 60×60 .

The first scan was done at 90 kV and 6 mA. The grayscale values for five different regions (labeled from A–E) were shown to be localized in the axial slice taken from the phantom, with each ROI represented as a square in a particular region. All the five ROIs were smooth and uniform throughout the slice (Fig. 7; upper left panel). The adjacent graph of noise uniformity/grayscale showed the standard deviation (SD) values of the five means beside the SD value of the noise level at the central region of the phantom (region A; Fig. 7, upper right panel). All these SD values were found to be 0 (Fig. 6).

The contrast resolution was also obtained in the same session. Each ROI was found to be located properly in its corresponding material area shown in a longitudinal slice. There were four different materials contained inside the contrast phantom (Fig. 7, lower left panel), and they were assigned the numbers from 0 to 3 to indicate the ROI for each material. Number 0 was for aluminum; number 1 was for bone equivalent resin; number 2 was for acrylic plastic; and number 3 was for air. The opacities of ROI 0 and ROI 1 (aluminum vs. bone equivalent resin) differed in contrast with the first being white (completely radiopaque) while the second was gray (partly radiolucent). Both ROI 0 and ROI 1 were different to ROI 2 and ROI 3, both of which were completely radiolucent (Fig. 7, lower left panel). A horizontal white line representing the test target plane was found to run across ROI 2 (as advised in the data sheet).

In the contrast resolution graph, the horizontal lines represent the average gray value of the four ROIs while the short bar perpendicular to the horizontal line is the SD of the average. The highest gray value was for ROI 0 (aluminum), which was 230.88 ± 2.49 ; for ROI 1 (bone equivalent resin) the gray value was 65.61 ± 1.67 , while ROI 2 (acrylic plastic) and ROI 3 (air) showed the same

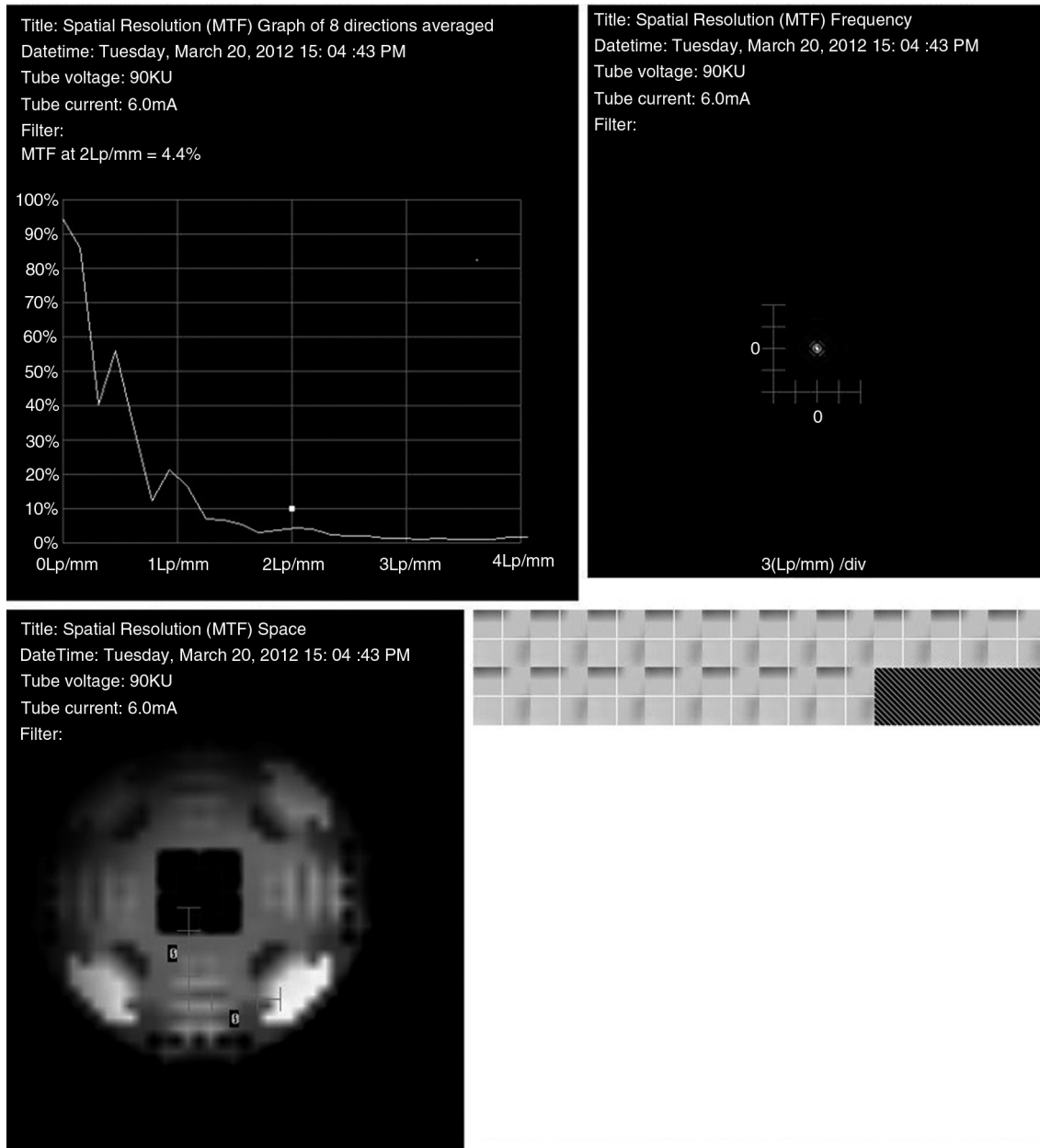


Fig. 4. MTF graph in 3D Accutomo 80 (60 × 60, 90 kv, 6 mA) to be 4.4% when set at 2 lp/mm (upper left panel). The object on which MTF value was assessed had a spatial frequency of 3 lp/mm (upper right panel) in the space inside the phantom (lower left panel). Axial slices of the object show the luminance intensity after receiving the X-ray signal; no artifacts were noticed (lower right panel).

value, that is, 31 ± 00 thus their line level was continuous (Fig. 7, lower right panel).

The second measurement was done at 80 kV and 7 mA while the FOV was kept the same, that is, 60 × 60. With this setting and as with the previous measurement, all the five ROIs (from A–E) appeared smooth and uniform in the axial plane of the phantom (Fig. 8, upper left panel). The SD of the noise uniformity and grayscale values of the five regions in the phantom was calculated as 0.67; while the SD of the noise value at the central region A was 0.52 (Figs. 6 and 8, upper right panel).

As in the previous session, the longitudinal section of the contrast phantom showed the four ROIs to be located properly in their corresponding material areas. By inspection, the opacities of ROI 0 and ROI 1 (aluminum vs. bone equivalent resin) showed the same degree of difference as previously, and both ROI 2 and ROI 3 were completely dark. The target plane was found, again, as a white line crossing ROI 2 (Fig. 8, lower left panel).

For the contrast resolution graph, no overlapping was seen among the different levels with the highest gray value was for ROI 0 (aluminum), which was 204.06 ± 2.72 ; for

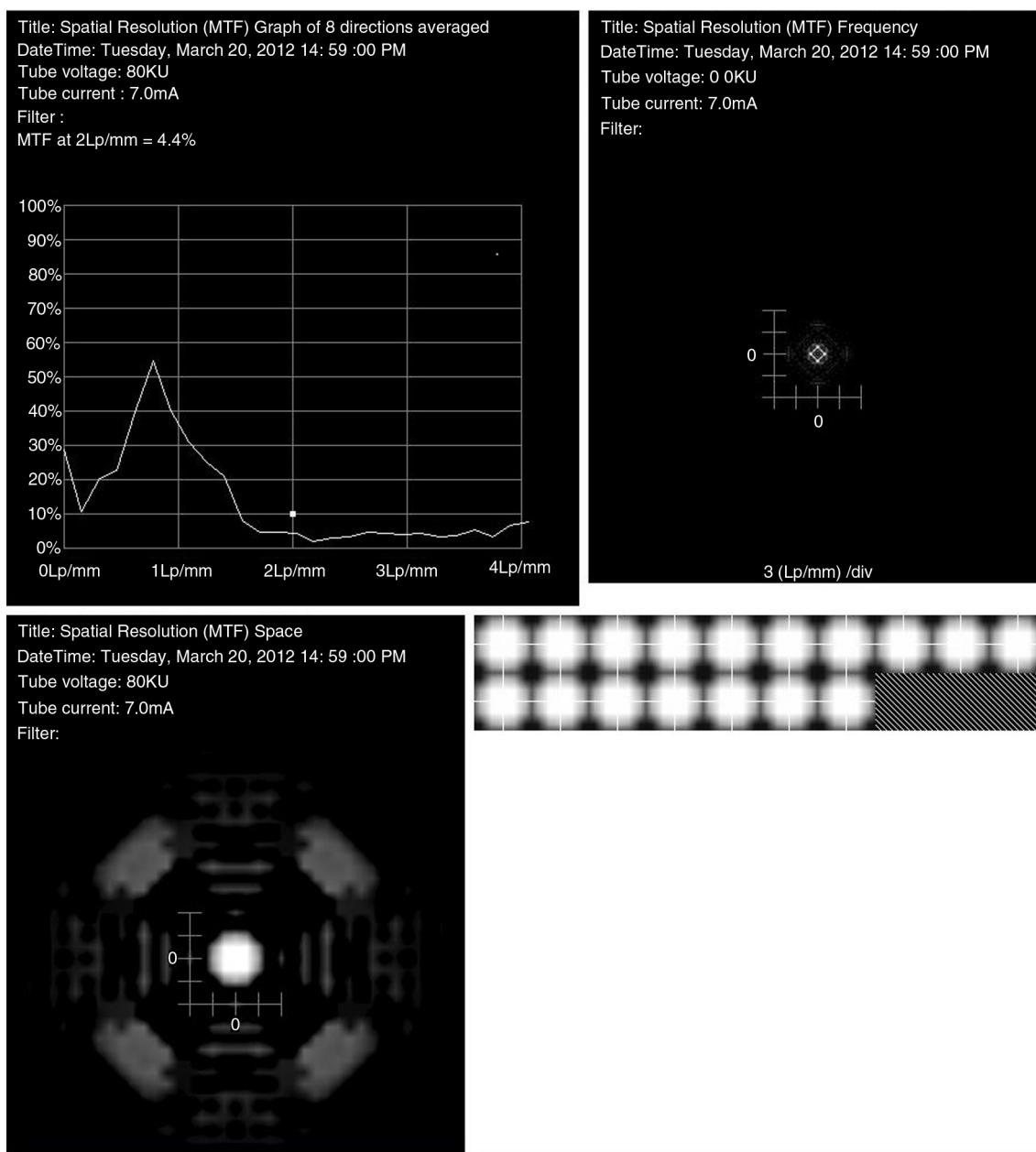


Fig. 5. MTF in 3D Accuitomo (60 × 60, 80 kv, 7 mA) to be 4.4% when set at 2 lp/mm (upper left panel). The object on which MTF value was assessed had a spatial frequency of 3 lp/mm (upper right panel) in the space inside the phantom (lower left panel). Axial slices of the object show the luminance intensity after receiving the X-ray signal; no artifacts were noticed (lower right panel).

ROI 1 (bone equivalent resin) the gray value was 68.05 ± 1.13 ; for ROI 2 (acrylic plastic) the gray value was 13.36 ± 0.61 ; and ROI 3 (air) showed nearly the same value, that is, 12.00 ± 0 (Fig. 8, lower right panel).

Radiation dose

The radiation dose was found to be of different values in the different locations of the TLD chips as shown in the tables. Each CBCT was scanned twice. Two parameters were changed in the CBCT unit: voltage (kV) and current

(mA); while the scan time and FOV were kept the same, that is, 17.5 sec and 80 × 80 mm, respectively.

With 3D Accuitomo 80, the first measurement process started with the setup of 80 kV and 7 mA and the phantom was scanned for 17.5 sec. The values were calculated for the effective dose. The effective dose values were found to range from 0.3 mSv (at position 9) to 0.54 mSv (at position 1; Table 1), with an average of 0.33 (SD ± 0.15).

In the second round, the voltage was increased up to 90 kV while the current was reduced to 6 mA, keeping the

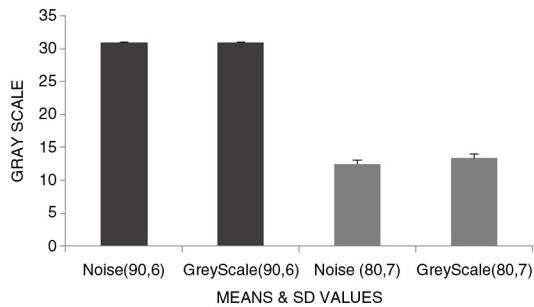


Fig. 6. A graph illustrating the means of grayscale values and SD value of the central region (for noise) in both measurements. The SD is shown as small vertical bars on the smaller columns, while the SD of longer columns was zero: 90 = 90 kV, 6 = 6 mA, 80 = 80 kV, 7 = 7 mA.

scan time and FOV the same. The figures obtained ranged from the minimum of 0.04 mSv (position 9) to 0.63 mSv (position 7) (Table 2), with an average of 0.34 (SD \pm 0.18). Using paired *t*-test analysis, no statistical significance was found in the difference of the values of the two scan doses ($p > 0.05$; Fig. 9).

With Scanora 3D, the first measurement was commenced with the FOV 75×100 , voltage value of 90 kV and 12.5 mA ampere, and the phantom was scanned for 4.3 sec. The smallest effective dose was 0.02 mSv (encountered in position 9), while the highest dose was 0.43 mSv (position 7; Table 3) with an average of 0.25 (SD \pm 0.12).

In the second measurement, the FOV was changed to 60×60 while all other parameters were kept the same. The resulting dose values ranged from 0.01 mSv (position 9) to 0.31 (position 1; Table 4) with an average of 0.12 (SD \pm 0.08). Statistically, the difference between these two sets of measurements, using paired *t*-test, was found significant ($p < 0.05$; Fig. 10).

Discussion

CBCT scanners come in different shapes and sizes. Although obtaining images of optimum contrast and resolution is a main target for oral health professionals, patient's safety against radiation remains a priority. A few studies have evaluated the quality of images taken with CBCT (19, 20) along with radiation dosimetry; our results seem to be somehow comparable assuming that our MTF values were the same as the standard, that is, 10%.

In the present study, the radiation doses of both CBCT units, that is, 3D Accuitomo 80 and Scanora 3D, were measured twice (the radiation dose of each unit was measured twice separately) using slightly different settings. The highest dose was noticed in both positions 1 and 7 seemingly because they occupy the most frontal locations in the phantom slice, thereby being most exposed to X-rays. Position 9 showed the least dosing values in both scans, probably due to its location in the center surrounded by more tissues. Overall, no significant differences were

found between the two dosing values in the two scans of 3D Accuitomo 80 ($p > 0.05$). Apparently, the nearly similar levels of doses found might be due to the changes of two important set-ups in reversed ways. The first scan session was done with higher amperage but less voltage than the second session. Therefore, any rise in the dose level due to higher current would be balanced by the lower voltage used. The same holds true in the second session but in an opposite way, that is, any rise in the dose value due to higher voltage would be balanced by lower amperage setting. However, small differences did exist between the two scans and that was due to the different mechanisms of the two physical parameters in influencing the radiation dose. A higher voltage renders the X-ray capable of penetrating the tissues more easily because the photons will possess higher energy. A higher current, in contrast, raises the number of photons emitted and thus increasing the radiation dose. This evokes the question as to what level both the CBCT unit voltage and amperage contribute individually to the radiation dose and also which produces the heavier load of the resulting X-ray. In our experiments, we always had to adjust between raising the voltage and lowering the amperage so as not to compromise the image quality. Some studies, for example, Jeong et al., showed that exposure time and tube amperage are the most significant in terms of modulating the radiation dose in CT imaging (21).

In Scanora 3D, changing only the FOV from 75×100 to 60×60 made all the dose values in the second setting (despite having a little more scan time) be lower (means 0.25 and 0.12, respectively) except at position 1 and the difference was negligible. Obviously, the reason for this difference resides in the fact that radiation delivered to objects in larger FOVs, as in the first setting, is more than in smaller fields (22). It was rational that pairing both scans of Scanora 3D yielded significant differences ($p < 0.05$) since we tested only one parameter, that is, FOV from a state of wider area of X-ray emission to a smaller one. The accompanying increase in the scan time, being very small, seems to have a trivial effect.

Interestingly, in all measurements, the doses on the left side of the phantom were the lowest. There are seemingly two logical reasons: either due to the peripherally positioned FOV or partial rotation. Since both units imply full rotation, the most likely reason lies in the peripheral location of the target FOV. Besides, the places 5, 6, 11, and 12 received much less radiation because they are not close to the surface. In other words, a part of the radiation has been absorbed before reaching them.

More interestingly, position 9 on the dosimetry phantom showed the least dose value in all four measurements, which might be due to its hiding location with equal bulks of tissue surrounding it from all sides.

To reduce the radiation dose to patients, the operator can manually adjust some of the machine settings, for

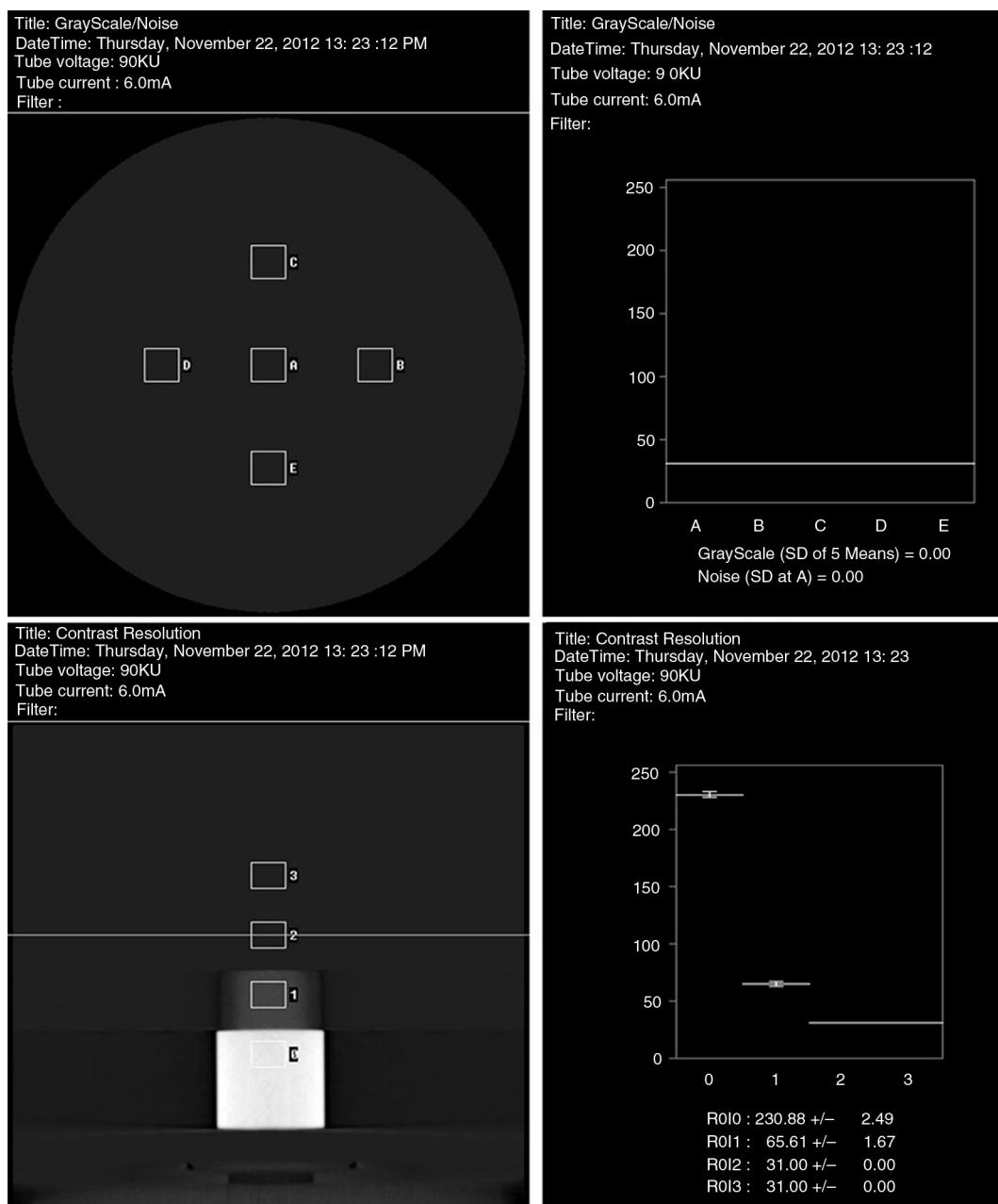


Fig. 7. Contrast measurement in 3D Accuitomo 80 (60 × 60, 90 kV, 6 mA) showing the uniformity/grayscale of five selected regions in the phantom (upper left panel), and the SD value of their five means besides the SD of the noise at the central region (upper right panel). The contrast resolution using four different materials in the phantom (lower left panel) was tested and the values are shown in the graph (lower right panel).

example, reducing exposure time and lowering the mA setting. However, following such a protocol may compromise the signal reaching the detector and thus the image quality (23).

The resultant X-ray doses of the two CBCT models in this experiment confirm the established theme that such organ-specific scanners are more conservative than the conventional CT systems in terms of exposing patients to radiation. Kalender et al. have introduced PC software for estimating the organ and effective doses of CT units,

and they showed the organ dose values of some previous studies in which the phantom head was among the different parts assessed by spiral CTs (24).

In clinical CBCT imaging, image quality is of paramount importance for the diagnostician to reach the precise entity of the disease and thus build a proper treatment plan for the patient. The quality of CT scan is influenced by four basic factors: contrast, spatial resolution, signal-to-noise ratio, and artifacts (13). However, only the first two factors were considered in the present measurements of

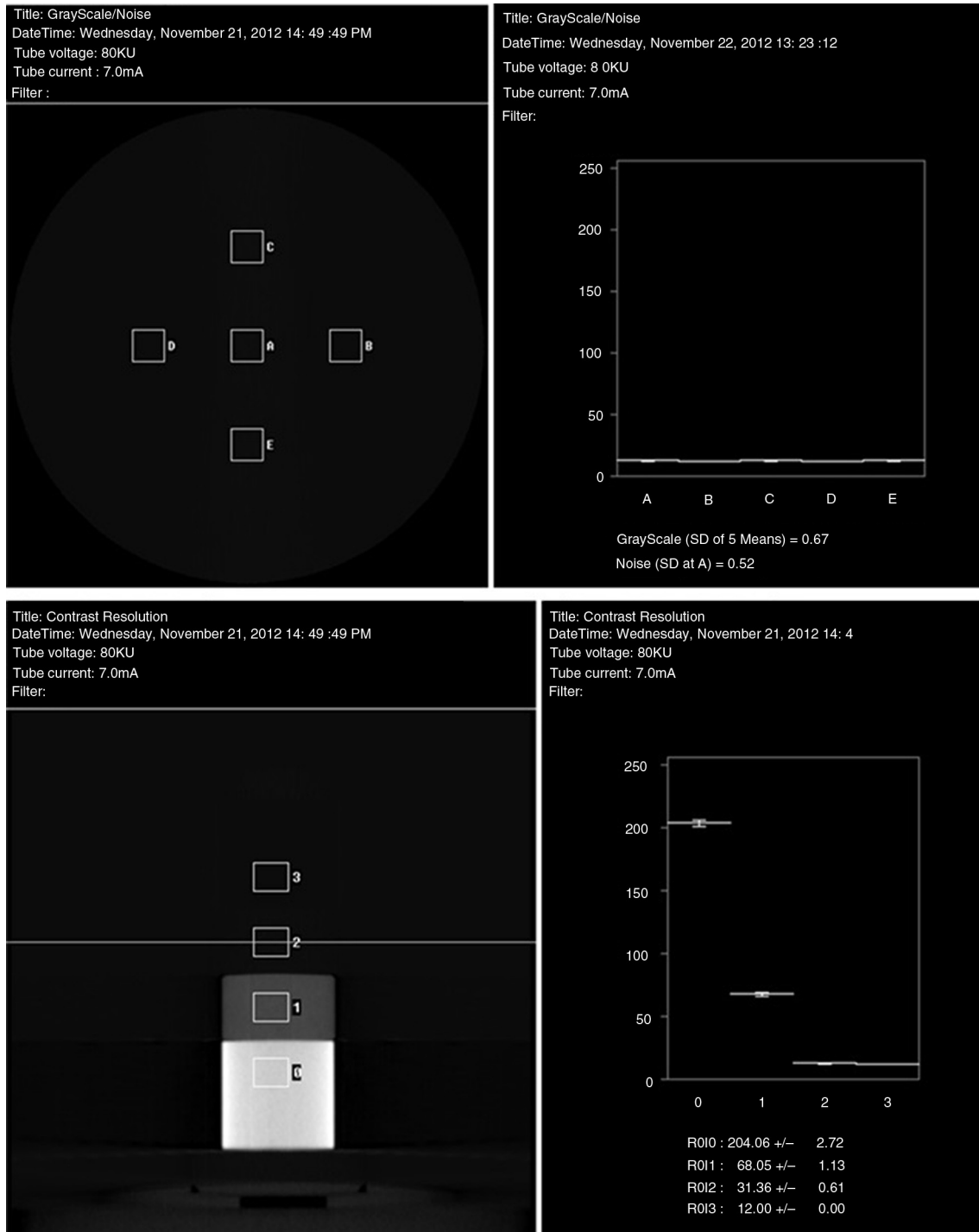


Fig. 8. Contrast measurement in 3D Accuitomo 80 (60 × 60, 80 kv, 7 mA) showing uniformity/grayscale of five selected regions in the phantom (upper left panel), and the SD value of their five means besides the SD of the noise at the central region (upper right panel). The contrast resolution using four different materials in the phantom (lower left panel) was tested and the values are shown in the graph (lower right panel).

this work. In addition, it was among the aims of this thesis plan to relate the radiation dose of 3D Scanora to its image quality, but unfortunately, as stated earlier, the unit had been taken away before conducting the measurements. The spatial resolution of an imaging system decides on

the ability of the imaging system to detect fine details in the image.

The second image quality factor assessed in 3D Accuitomo 80 was contrast (including noise and uniformity/grayscale). In physics, contrast is the difference between

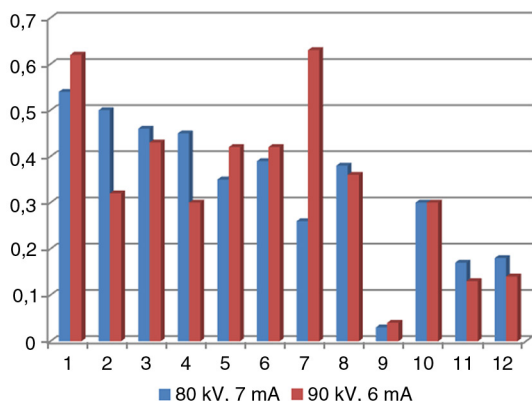


Fig. 9. The graphic distribution of the radiation doses in the two scans of 3D Accuitomo 80. It can be seen that the values in the two scans are generally similar and, using paired *t*-test, no significant differences were found ($p > 0.05$).

the signal received from the object and that of its background (25), and the more this difference is, the better the object can be perceived.

Even though certain modifications have been attempted on CBCT, for example, 3XD multi-image micro-CT and found to be of considerable enhancement to the device performance in producing better image quality than multi-slice CT (26), such CBCTs units are still in need of improvement to their contrast ability compared with their counterpart systemic CTs.

To determine the contrast perceptibility, a contrast phantom consisting of different materials, which resemble the intensity of the human tissues in the dentofacial complex, was used. It is well known that CBCT units suffer from poor soft tissue contrast and they are mainly meant for visualizing the dental hard structures (27). The contrast parameter was scanned twice using the same

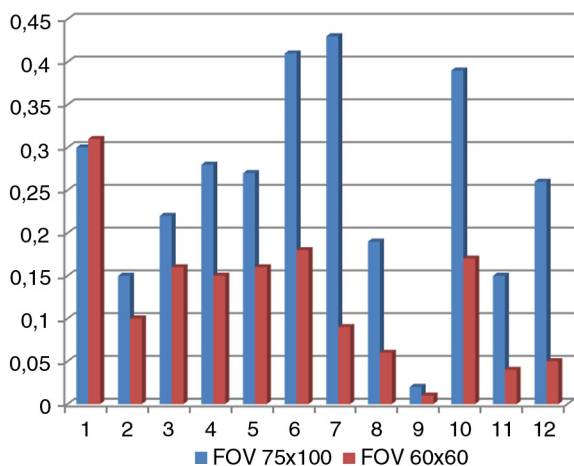


Fig. 10. The graphic distribution of the radiation dose value of the Scanora 3D in the two sessions of changing FOVs. It is obvious that the values of the wider FOV (75 × 100) tend to be higher than the 60 × 60 FOV ($p < 0.05$).

Table 1. The radiation dose values of 3D Accuitomo 80: field: 80 × 80, voltage: 80 kV, current: 7 mA, and duration: about 17.5 sec

Place on phantom	Dose (mSv)
1	0.54
2	0.50
3	0.46
4	0.45
5	0.35
6	0.39
7	0.26
8	0.38
9	0.03
10	0.30
11	0.17
12	0.18

settings which were used in a spatial resolution test. The uniformity of different spots on a cross-sectional slice of the phantom was evaluated to measure the ability of CBCT to produce uniform images across the layer of the object with homogenous density in a particular FOV. The image displayed did not suffer any distortion in both sessions. These five ROIs were also assessed for noise and level of grayscale in the resultant image. Interestingly, in the setting of higher voltage and less amperage, the SD of the central ROI (which is a measure of the noise) equaled zero, slightly less than the second setting. It should be noticed that our machine FOV, scan time (17.5 sec and 360°) and, hence, the voxel size (0.125 mm) were all the same in both measurements. This leaves us to believe that the loss of noise taken from the acrylic layer was due to the higher voltage and lower current used. However, an important parameter known as contrast to noise ratio

Table 2. The radiation dose values of 3D Accuitomo 80: field: 80 × 80; voltage: 90 kV; current: 6 mA; and duration: about 17.5 sec

Place on phantom	Dose (mSv)
1	0.62
2	0.32
3	0.43
4	0.30
5	0.42
6	0.42
7	0.63
8	0.36
9	0.04
10	0.30
11	0.13
12	0.14

Table 3. The radiation dose values of Scanora 3D under the following parameters: field: 75×100 ; voltage: 90 kV; current: 12.5 mA; and duration: 4.13 sec

Place on phantom	Dose (mSv)
1	0.30
2	0.15
3	0.22
4	0.28
5	0.27
6	0.41
7	0.43
8	0.19
9	0.02
10	0.39
11	0.15
12	0.26

(CNR) can give a more reliable picture about the image quality than image noise (28), but this requires a well-fabricated phantom consisting of the studied object and control material (usually water). When this is achieved, CNR can be calculated (29).

In both measurements, 3D Accuitomo 80 imaging showed very good contrast of hard materials, that is, aluminum and bone equivalent resin. Less contrast perception was, however, noticed in case of low-density materials where the radiolucency of both plastic and air was exactly the same and nearly the same in the first and second setting, respectively. This is, again, explained by the inherent limitation of CBCT to offer good soft tissue contrast in clinical imaging, thereby yielding weak perceptual differentiation of tissues with low density, for example, muscular or fibrous tissues.

Table 4. The radiation dose values of Scanora 3D under the following parameters: field: 60×60 ; voltage: 90 kV; current: 12.5 mA; and duration: 4.5 sec

Place on phantom	Dose (mSv)
1	0.31
2	0.10
3	0.16
4	0.15
5	0.16
6	0.18
7	0.09
8	0.06
9	0.01
10	0.17
11	0.04
12	0.05

Conclusions

From our perspective, the present results have successfully fulfilled the original aims of this study. For instance, changing the voltage and current settings in a counter-active manner does not seem to affect the spatial resolution of the image produced, provided that the image mode (FOV) is kept the same. Moreover, no artifacts tend to be formed by such a manipulation. In addition, with the second parameter of image quality, a very small difference was noticed. Setting the tube voltage at 80 kV and its current at 7 mA resulted in a very small noise level and less contrast resolution between two hard materials with different densities. Raising the tube voltage and reducing the current (i.e. 90 kV and 6 mA) abolished such a noise and widened the grayscale gap difference a little more (slightly improving contrast). Moreover, for the dosimetry, having a higher tube voltage and lower current of 3D Accuitomo 80 resulted in a trivial rise in the doses received. In Scanora 3D, changing the FOV, from wider to narrower, yielded a substantial reduction in the radiation doses. As a conclusion, digital imaging represents one of the most crucial diagnostic instruments for oral health professionals. Therefore, with superior caution of patient's safety against lethal radiation, significant improvement in the diagnosis outcomes and treatment plans of dental and maxillofacial disorders would become feasible.

According to present results, the authors recommend using 3D Accuitomo 80 rather than Scanora 3D products whenever the choice is based on these two CBCT machines.

Conflict of interest and funding

The authors have not received any funding or benefits from industry or elsewhere to conduct this study.

References

- Dawood A, Patel S, Brown J. Cone beam CT in dental practice. *Br Dent J.* 2009; 207: 23–8.
- Grunheid T, Kolbeck Schieck JR, Pliska BT, Ahmad M, Larson BE. Dosimetry of a cone-beam computed tomography machine compared with a digital x-ray machine in orthodontic imaging. *Am J Orthod Dentofacial Orthop.* 2012; 141: 436–43.
- Aoki N, Toyofuku T, Komiya K. Cerebellar infarction. *Neuropediatrics.* 1986; 17: 124–8.
- Mozzo P, Procacci C, Tacconi A, Martini PT, Andreis IA. A new volumetric CT machine for dental imaging based on the cone-beam technique: preliminary results. *Eur Radiol.* 1998; 8: 1558–64.
- Arai Y, Tammsalo E, Iwai K, Hashimoto K, Shinoda K. Development of a compact computed tomographic apparatus for dental use. *Dentomaxillofac Radiol.* 1999; 28: 245–8.
- Dugal R, Gupta AK, Musani SI, Kheur MG. Cone beam computed tomography: a review. *Univ Res J Dent.* 2011; 1: 30–7.
- Scarfe WC, Farman AG. What is cone-beam CT and how does it work? *Dent Clin North Am.* 2008; 52: 707–30, v.

8. Joshi P, Lele V, Gandhi R. Fluorodeoxyglucose positron emission tomography-computed tomography scan and nuclear magnetic resonance findings in a case of Stewart-Treves syndrome. *J Cancer Res Ther.* 2011; 7: 360–3.
9. Joshi P, Lele V, Gandhi R. Incidental detection of clinically occult follicle stimulating hormone secreting pituitary adenoma on whole body 18-fluorodeoxyglucose positron emission tomography-computed tomography. *Ind J Nucl Med.* 2011; 26: 34–5.
10. Gupta R, Grasruck M, Suess C, Bartling SH, Schmidt B, Stierstorfer K, et al. Ultra-high resolution flat-panel volume CT: fundamental principles, design architecture, and system characterization. *Eur Radiol.* 2006; 16: 1191–205.
11. Yan XH, Leahy RM. Derivation and analysis of a filtered backprojection algorithm for cone beam projection data. *IEEE Trans Med Imaging.* 1991; 10: 462–72.
12. Vassileva J. A phantom for dose-image quality optimization in chest radiography. *Br J Radiol.* 2002; 75: 837–42.
13. Goldman LW. Principles of CT: radiation dose and image quality. *J Nucl Med Technol.* 2007; 35: 213–25; quiz 226–8.
14. Droege RT, Morin RL. A practical method to measure the MTF of CT scanners. *Med Phys.* 1982; 9: 758–60.
15. Butt A, Mahoney M, Savage NW. The impact of computer display performance on the quality of digital radiographs: a review. *Aust Dent J.* 2012; 57(Suppl 1): 16–23.
16. Sharma DS, Sharma SD, Sanu KK, Saju S, Deshpande DD, Kannan S. Performance evaluation of a dedicated computed tomography scanner used for virtual simulation using in-house fabricated CT phantoms. *J Med Phys.* 2006; 31: 28–35.
17. Suomalainen A, Kiljunen T, Käser Y, Peltola J, Korttesniemi M. Dosimetry and image quality of four dental cone beam computed tomography scanners compared with multislice computed tomography scanners. *Dentomaxillofac Radiol.* 2009; 38: 367–78.
18. Sawyer LJ, Whittle SA, Matthews ES, Starritt HC, Jupp TP. Estimation of organ and effective doses resulting from cone beam CT imaging for radiotherapy treatment planning. *Br J Radiol.* 2009; 82: 577–84.
19. Watanabe H, Honda E, Kurabayashi T. Modulation transfer function evaluation of cone beam computed tomography for dental use with the oversampling method. *Dentomaxillofac Radiol.* 2010; 39: 28–32.
20. Araki K, Maki K, Seki K, Sakamaki K, Harata Y, Sakaino R, et al. Characteristics of a newly developed dentomaxillofacial X-ray cone beam CT scanner (CB MercuRay): system configuration and physical properties. *Dentomaxillofac Radiol.* 2004; 33: 51–9.
21. Jeong DK, Lee SC, Huh KH, Yi WJ, Heo MS, Lee SS, et al. Comparison of effective dose for imaging of mandible between multi-detector CT and cone-beam CT. *Imaging Sci Dent.* 2012; 42: 65–70.
22. Pauwels R, Beinsberger J, Collaert B, Theodorakou C, Rogers J, Walker A, et al. Effective dose range for dental cone beam computed tomography scanners. *Eur J Radiol.* 2012; 81: 267–71.
23. Hatcher DC. Operational principles for cone-beam computed tomography. *J Am Dent Assoc.* 2010; 141: 3S–6S.
24. Kalender WA, Schmidt B, Zankl M, Schmidt M. A PC program for estimating organ dose and effective dose values in computed tomography. *Eur Radiol.* 1999; 9: 555–62.
25. Barnes JE. Characteristics and control of contrast in CT. *Radiographics.* 1992; 12: 825–37.
26. Hashimoto K, Kawashima S, Araki M, Iwai K, Sawada K, Akiyama Y. Comparison of image performance between cone-beam computed tomography for dental use and four-row multidetector helical CT. *J Oral Sci.* 2006; 48: 27–34.
27. Chan M, Yang J, Song Y, Burman C, Chan P, Li S. Evaluation of imaging performance of major image guidance systems. *Biomed Imaging Interv J.* 2011; 7: e11.
28. Kalender WA, Deak P, Kellermeier M, van Straten M, Vollmar SV. Application- and patient size-dependent optimization of x-ray spectra for CT. *Med Phys.* 2009; 36: 993–1007.
29. Bechara B, McMahan CA, Geha H, Noujeim M. Evaluation of a cone beam CT artefact reduction algorithm. *Dentomaxillofac Radiol.* 2012; 41: 422–8.